Mechanics of Materials 41 (2009) 764–776

Contents lists available at ScienceDirect

Mechanics of Materials

journal homepage: www.elsevier.com/locate/mechmat

Comparisons of physical experiment and discrete element simulations of sheared granular materials in an annular shear cell

Shunying Ji [a,*], Daniel M. Hanes [b], Hayley H. Shen [c]

[a] State Key Laboratory of Structural Analysis for Industrial Equipment, Dalian University of Technology, Dalian 116023, China
[b] USGS Pacific Science Center, 400 Natural Bridges Drive, Santa Cruz, CA 95060, USA
[c] Civil and Environmental Engineering, Clarkson University, Potsdam, NY 13699-5710, USA

ARTICLE INFO

Article history:
Received 12 January 2009

ABSTRACT

In this study, we report a direct comparison between a physical test and a computer simulation of rapidly sheared granular materials. An annular shear cell experiment was conducted. All parameters were kept the same between the physical and the computational systems to the extent possible. Artificially softened particles were used in the simulation to reduce the computational time to a manageable level. Sensitivity study on the particle stiffness ensured such artificial modification was acceptable. In the experiment, a range of normal stress was applied to a given amount of particles sheared in an annular trough with a range of controlled shear speed. Two types of particles, glass and Delrin, were used in the experiment. Qualitatively, the required torque to shear the materials under different rotational speed compared well with those in the physical experiments for both the glass and the Delrin particles. However, the quantitative discrepancies between the measured and simulated shear stresses were nearly a factor of two. Boundary conditions, particle size distribution, particle damping and friction, including a sliding and rolling, contact force model, were examined to determine their effects on the computational results. It was found that of the above, the rolling friction between particles had the most significant effect on the macro stress level. This study shows that discrete element simulation is a viable method for engineering design for granular material systems. Particle level information is needed to properly conduct these simulations. However, not all particle level information is equally important in the study regime. Rolling friction, which is not commonly considered in many discrete element models, appears to play an important role.

1. Introduction

Since its initial development by Cundall and Strack (1979) the discrete element (DE) simulation method has been widely used to investigate the physics of granular materials. However, to be accepted by industry as a viable alternative to physical tests, DE simulations must be validated. Many physical tests of granular materials have been carried out in a variety of geometries. A partial list includes annular shear cells (e.g. Savage and Sayed, 1984; Hanes and Inman, 1985; Craig et al., 1987; Miller et al., 1996; Ladipo and Puri, 1997; Hsiau and Jang, 1998; Qin, 2000; Tsai and Gollub, 2004), tumbling mills (e.g. Venugopal and Rajamani, 2001; Cleary et al., 2003), silo flow (e.g. Vanel et al., 2000; Yang and Hsiau, 2001) and incline flows (e.g. Azanza et al., 1999; Pouliquen, 1999; Hanes and Walton, 2000; Jop et al., 2006).

Among these geometries, rotating cylinder shear cells provide the simplest flow regime. This type of shear cell was first reported by Bagnold (1954), in which the annular space between an inner stationary cylinder and an outer rotating cylinder was filled with granular materials. Since then different shear mechanism, with velocity gradient either axially oriented or radially oriented, have been

* Corresponding author.
E-mail addresses: jisy@dlut.edu.cn (S. Ji), dhanes@usgs.gov (D.M. Hanes), hhshen@clarkson.edu (H.H. Shen).

0167-6636/$ - see front matter © 2009 Elsevier Ltd. All rights reserved.
doi:10.1016/j.mechmat.2009.01.029

utilized to determine the stress and shear rate relations in granular materials (Savage and Sayed, 1984; Hsiau and Jang, 1998; Howell et al., 1999; Mueth et al., 2000; Qin, 2000; Luding, 2006). The annular shear cell differs from traditional shear devices used in soil mechanics such as the direct shear or the tri-axial cells in that for granular flows much higher shear rate (as well as post failure) conditions are of interest. Such conditions are commonly found in dynamic granular systems in industry and in nature.

Direct comparisons between physical and computer simulated granular flows are few and limited to kinematic variables (e.g. Venugopal and Rajamani, 2001). To rigorously validate the applicability of DE simulations in engineering applications, comparisons of the force field are needed. In this study, we use an annular shear cell geometry and two different granular materials to establish the comparison between the physical and DE simulation results.

2. The physical experiment

The annular shear cell used in this study was the same as reported in Hanes and Inman (1985) and Qin (2000). A sketch of this shear cell is reproduced in Fig. 1. The top and bottom of the shear cell were roughened with particles densely glued on the surface. The side walls were smooth.

The experimental procedure began with pouring a measured amount of granular materials into the circular trough of the shear cell, placing the top cover into the filled trough, applying a desired counter weight to the top cover to produce a prescribed normal load N, setting the rotating bottom to a desired speed, and recording the resulting resisting torque on the fixed top cover. A set of RPM and normal load N was used on two different granular materials: glass and Delrin. We believe both the experiments and the simulations are the first such results reported for Delrin particles. The test matrix and the material properties of the granular materials are given in Table 1.

Table 1
Materials used in the physical tests.

Material		Glass	Delrin
Mean particle diameter	D_p	3 mm	3.2 mm
Boundary particle diameter	D_b	3 mm	3 mm (glass)
Outside radius of shear cell	r_2	146 mm	146 mm
Inside radius of shear cell	r_1	102 mm	102 mm
Height of the shear call	H	12.11–16.66 mm	22.6–23.3 mm
Sphere–sphere friction coefficient	μ_{p-p}	0.177	0.22
Sphere–wall friction coefficient	μ_{p-w}	0.2	0.25
Sphere–sphere restitution coefficient	e_{p-p}	0.972	0.97
Sphere–wall restitution coefficient	e_{p-w}	0.97	0.95
Particle density	ρ	2946 kg/m^3	1300 kg/m^3
Rotation speed	n	2–170 rpm	2–27 rpm
Normal stress	σ_{zz}	0.6–2.1 kPa	360–926 Pa
Total mass of shear material	M	0.675 kg total	0.481 kg total

In Table 1, the material properties of the particles, and the particle–particle and particle–wall interaction parameters were obtained from Foerster et al. (1994) and Lorenz et al. (1997) in which only partial tables of tested materials were listed. The full table of tested materials may be obtained from Louge (personal communication).

During these tests, the amount of granular materials was fixed but the top cover can move up or down in reaction to the internal normal stress and the applied counter weight. In this way, the solid fraction inside the shear cell fluctuated slightly during the rotation but the normal load on the granular materials was equal to the prescribed value.

3. The numerical simulation

In order to model the particles as accurately as possible, we adopted a soft particle interaction algorithm as

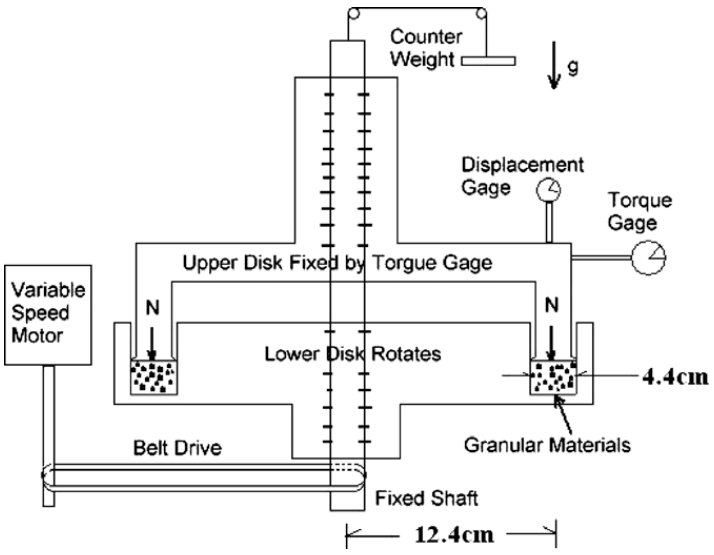

Fig. 1. Schematics of the annular shear cell.

described in the DE literature (Cundall and Strack, 1979; Babic et al., 1990; Zhang and Rauenzahn, 2000; Campbell, 2002). The particles were placed in a numerically defined shear cell with the same dimensions as used in the physical experiment. A hexagonal pattern was used to form the initial packing. After a short transient period, the shearing response became independent of the initial condition. The boundary particle pattern posed a problem. Because in the physical tests the boundary particles were manually attached to the top and bottom surfaces to form a dense packing pattern, the inherent irregularity could not be exactly reproduced numerically. We tried several different ways to produce the boundary and found that as long the packing was sufficiently dense, the effect of packing pattern had little influence on the results. We thus decided to use a radially hexagonal packing as shown in Fig. 2a to produce the top and bottom surfaces. This radially hexagonal packing was formed with a regular Cartesian hexagonal array and remapped from the (x,y) plane to the corresponding (r,θ) plane. The packing of boundary particles in the physical experiments was also close-packed and nearly hexagonal, though without the remapping into the radial plane.

In DE simulations the challenge is the computing time. For the amount of mass and particle size used in the physical experiment, the simulation of the fastest shear rate would take several months using the currently available desktop computers. Two techniques have been used to speed up the simulation: reducing the space and softening the particles. As shown in Fig. 2b, the actual simulation domain was a 30° wedge with periodic boundary conditions at the wedge boundaries. The simulation time step is controlled by the binary contact time t_{bc} between two particles. The accuracy of the simulation requires Δt be a small fraction of t_{bc}. In our simulations $\Delta t = t_{bc}/50$. Let the particle mass be m, it can be shown that (Babic et al., 1990)

$$t_{bc} = \frac{\pi}{\sqrt{(2K_n/m)(1-\zeta_n^2)}} \tag{1}$$

where $K_n \sim ED$ and ζ_n is related to the restitution coefficient e through

$$\zeta_n = \frac{-\ln e}{\sqrt{\pi^2 + \ln^2 e}} \tag{2}$$

Hence the stiffer the particles are, the smaller the time step, and the longer the simulation time. To overcome this problem, we tested several different "artificial stiffness" values to examine their effects on the results.

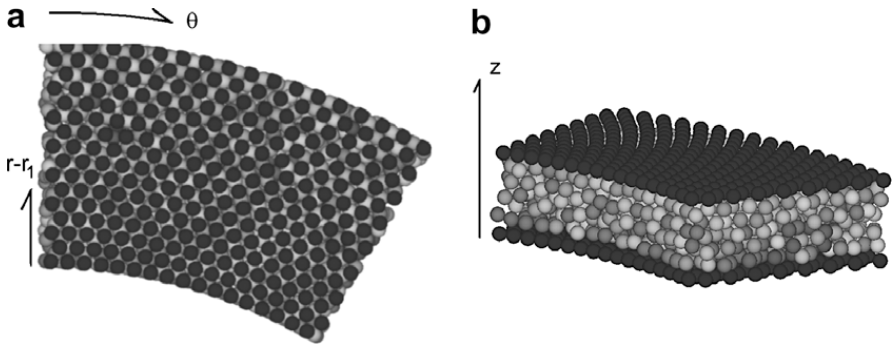

Fig. 2. The (a) boundary and (b) interior packing of a simulated 30° shear cell. In which r_1 is the radius of the inner circle.

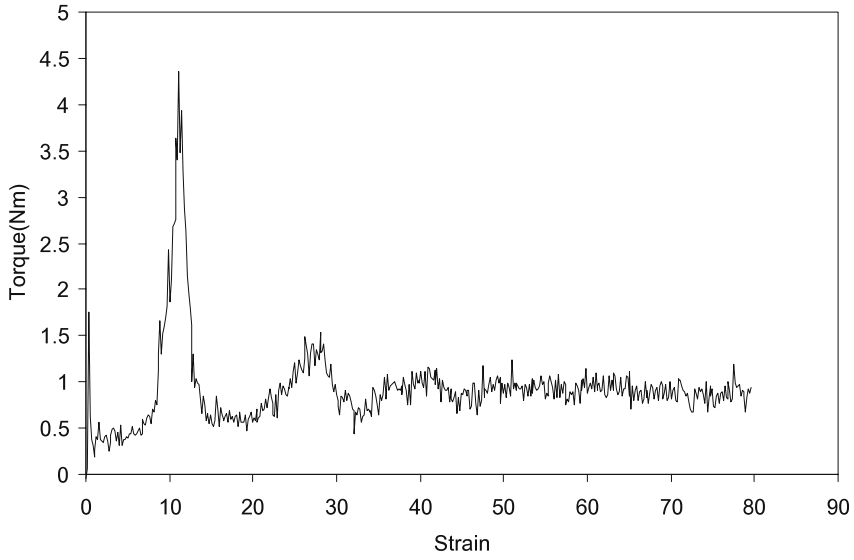

Fig. 3. Simulated torque on the top cover under a rotation velocity of 120 rpm and a normal load of 18.5 N.

The contact force model used was the common linear spring and dashpot model as described in Babic et al. (1990) and Campbell (2002), where $F = F_{spring} + F_{dashpot} = K\delta + \zeta\,\dot{\delta}$ with δ the particle–particle overlap and $\dot{\delta}$ the relative velocity of approach between two contacting particles. The stiffness parameter is related to the particle Young's modulus E as $K = \pi DE/4$. This model was applied to both normal and tangential directions of contact with the same assumed parameters in both directions.

The DE simulations used the exact same parameter values as shown in Table 1 except the stiffness. The real Young's modulus for glass is in the range of 70–100 GPa. Delrin is lower but with the same order of magnitude. A range of the "computational stiffness" is used in the simulation. For glass particles, stiffness values from 8.5×10^5 to 8.5×10^8 were tested. Since the results were insensitive to the stiffness, for the Delrin case only one Young's modulus value of 4.2×10^6 was used.

4. Comparisons between the physical and numerical data

Using the glass particles with a mono-size distribution, the shear process in the shear cell was simulated with the DE model in a 30° computational domain as shown as Fig. 2. The time series of the simulated torque on the top cover of the shear cell for a rotational speed of 120 rpm is plotted in Fig. 3. In this and subsequent figures, the stain γ is defined as the product of strain rate $\dot{\gamma}$ and time, where $\dot{\gamma} = \frac{r_1+r_2}{60z_0}\pi n$, and r_1, r_2 are the inner and outer radius of the shear cell, respectively, z_0 is the thickness of the granular materials in the shear cell, and n is the rotation speed of shear cell in rpm. The effective applied normal force (the weight of the top cover minus the counter weight) for the case shown was 18.5 N, and Young's modulus was 8.5×10^6 Pa. This result shows a peak in the torque at the beginning before it drops off to a steady state, where

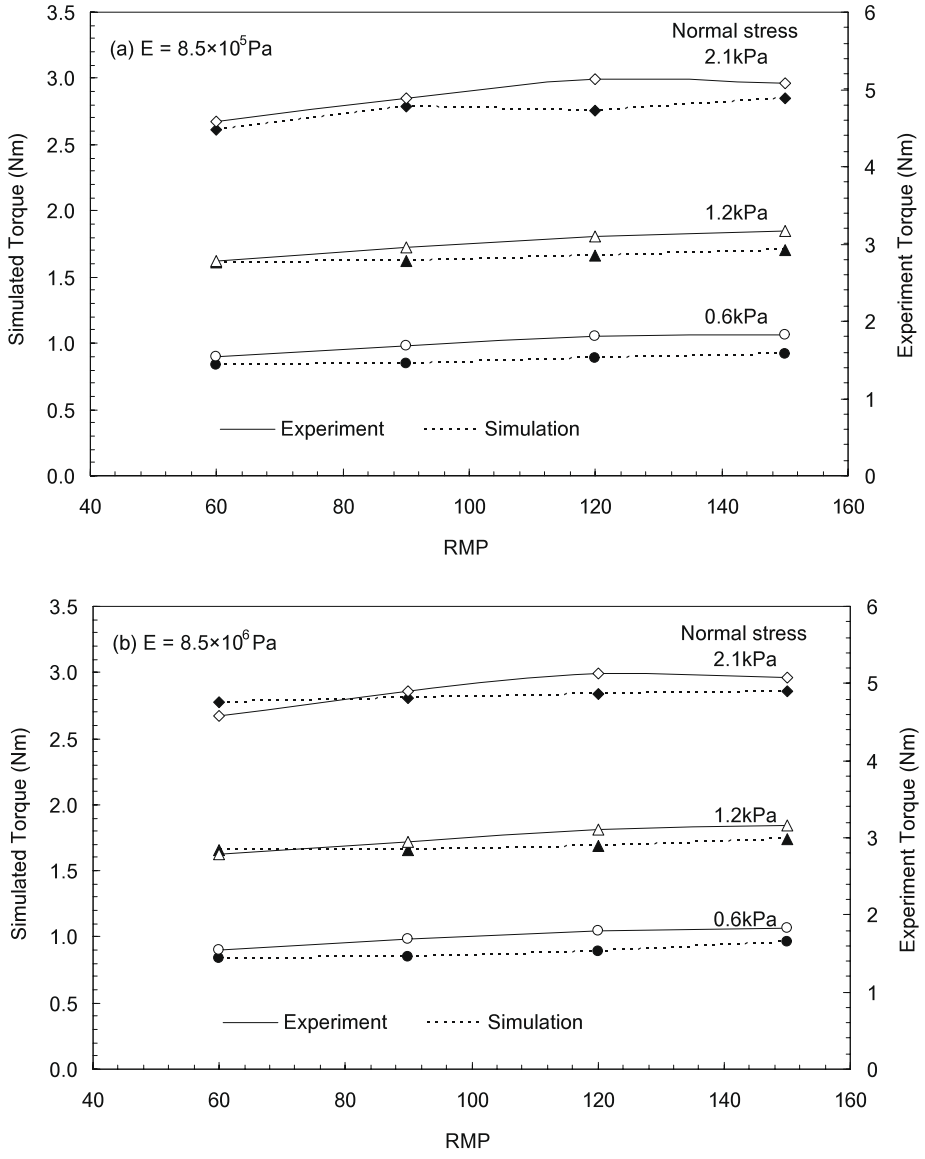

Fig. 4. Numerical results of glass particles in the shear cell with different Young's modulus. (a) $E = 8.5\times10^5$ Pa; (b) $E = 8.5 \times 10^6$ Pa. Left vertical scale for simulation and right for experimental results.

the averaged value is 0.92 Nm. With various rotation velocities and normal forces as listed in Table 1, the simulated steady state torques acting on the top cover are compared with the physical data in Fig. 4. Note in Fig. 4 two vertical scales are used to better show the variations, because the simulation results are roughly half the value of the experimental data.

From Fig. 4, particle stiffness appears to have little effect on the simulation results. We tried two more cases with $E = 8.5 \times 10^7$ Pa and $E = 8.5 \times 10^8$ Pa. The results for all these cases are given in Table 2. It is clear that particle stiffness does not affect the results for the cases tested.

The shearing of Delrin particles is also simulated. In Fig. 5, these results are given for $E = 4.2 \times 10^6$ Pa only.

All simulations used IBM single processor computers with 3 GHz Pentium processors and 1 GB RAM. The case with $E = 8.5 \times 10^5$ Pa and a 30° wedge took around 1-h of computing time. The computing time increases with $\sqrt{E/\rho D_p^2}$.

5. Discussion

The comparison between the physical experiment and the computer simulation is consistent among all cases studied. The qualitative agreement is good but the discrepancies are quantitatively significant. For all cases investigated, the simulated torque is about 1/2 of the measured for both materials. The first plausible source of the difference is in selecting the material parameters. Particle size and density are straightforward parameters with very small measurement error. Particle stiffness is an insensitive parameter as shown from the data given in Fig. 4 and Table 2. The remaining possibilities include:

1. boundary packing effect;
2. particle size distribution;
3. contact sliding friction and damping coefficient;
4. rolling friction;
5. contact force model;
6. combining sliding and rolling friction effects.

We investigated each of these possibilities and discuss these effects below.

Table 2
The simulation results for glass particles.

n (rpm)	Normal load N (N)	Experiment	Simulation	
		T (Nm)	E (Pa)/8.5	T (Nm)
120	18.50	1. 80	10^5	0.891
			10^6	0.886
			10^7	0.916
			10^8	0.891
150	37.85	3.17	10^5	1.705
			10^6	1.736
			10^7	1.731
			10^8	1.708

5.1. Boundary packing effect

Two types of boundaries were constructed to test the effect of boundary packing. One was called "loose" and the other "dense". Both types of packing began with a normal hexagonal pattern in the Cartesian coordinate as shown in Fig. 6. In each case the actual packing density was controlled by the parameter C_w described in Fig. 6.

The Cartesian to polar coordinate transformation was then performed to map the particles to the annular shear cell geometry in the following way:

$$x = (r_1 + yy)\cos\left(\frac{xx}{r_1 + yy}\right), \quad y = (r_1 + yy)\sin\left(\frac{xx}{r_1 + yy}\right) \tag{3}$$

Examples of the loose packing with $C_w = 0.8$ and dense packing with $C_w = 1.0$ are shown in Fig. 7(a) and (b), respectively.

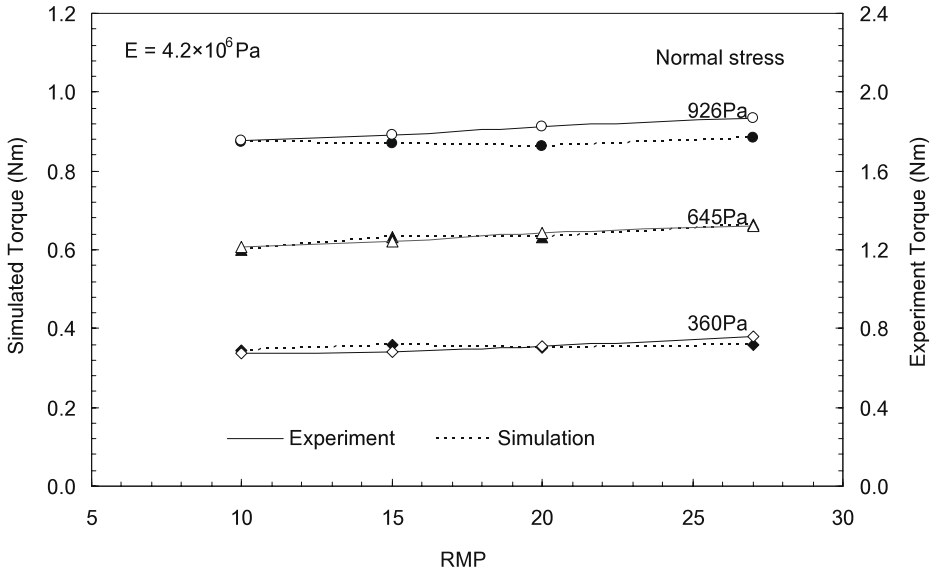

Fig. 5. Comparison for the Delrin case. Left vertical scale for simulation and right for experimental results.

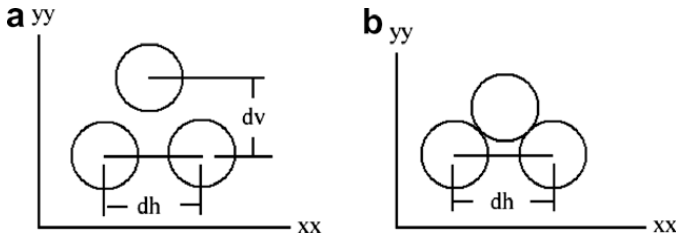

Fig. 6. The (a) loose and (b) dense packing in the Cartesian plane, where $dh = D_w/\sqrt{C_w}$ for both cases. The vertical separation $dv = dh\sqrt{3}/2$ in the loose packing and there is no gap between layers in the yy-direction in the dense packing.

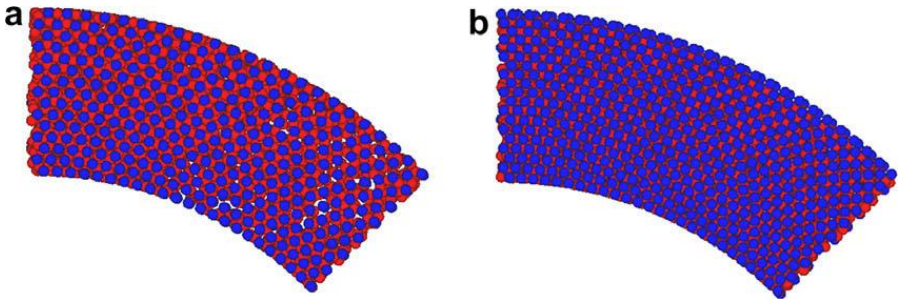

Fig. 7. The boundary packing where (a) loose pack with $C_w = 0.8$ and (b) dense pack with $C_w = 1.0$. Notice that $C_w = 1.0$ corresponds to no gaps for the inner most layer.

A test was made with a 30° wedge. Two different packings, the dense one with $C_w = 1.0$ and the loose one with $C_w = 0.8$. Both cases used the same material parameters $\mu_{p-p} = 0.177$, $\mu_{p-w} = 0.2$ and $e_{p-p} = e_{p-w} = 0.97$ and identical conditions other than the boundary condition. The normal load was 37.83 N, and the rotation speed was 120 rpm. The torque on the top surface was found to be 1.63 for the dense case and 1.65 for the loose case, where torque values were averages for the steady state portion corresponding to strain values = [40,60]. These average values are robust. For example, when averaged over a strain range = [60,80], we obtain 1.67 for the dense case, and 1.64 for the loose case. The evolution of the torques with respect to strain is given in Fig. 8. These results indicate that the boundary packing has little influence on the shear resistance for the range of packing tested. This finding is consistent with a more thorough study of the boundary effect in a 2D granular shear flow (Campbell, 1993), in which uniformly spaced disks were glued on the boundaries to produce roughness. A large range of spacing from 0 to infinity was investigated. It was found that for moderate values of spacing between glued disks the effect on the internal stress was minor.

5.2. Particle size distribution

We next tested particle size distribution. Knowing that despite the strict particle size selection when conducting

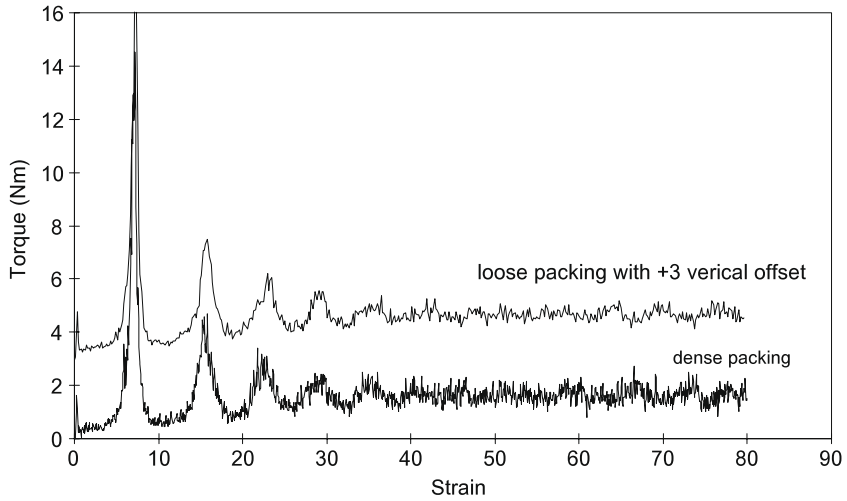

Fig. 8. The torque on the top surface of the shear cell. The values for the dense packing case are added by 3 in order to separate the two curves.

the physical experiment, some randomness might still exist. We thus assumed a uniformly distributed size with ±0.2 mm from the mean diameter, roughly a 7% deviation from the mean. The simulated results for both glass and Delrin materials are plotted in Fig. 9. These results do not change the torque values by more than 10%.

5.3. Sliding friction and damping coefficient

The restitution and sliding friction coefficients were not directly measured. They were obtained from previously reported values in the literature as discussed earlier. As long as the manufacture procedure for these materials remains the same, the material properties should not change much. In fact, previous studies of simple shear granular materials have shown that bulk friction is insensitive to the restitution coefficient at high concentration over the range of shear rate studied here (Campbell, 2002). However, sliding friction can change the bulk friction significantly for constant solid fraction test in the range of μ_{p-p}, $\mu_{p-w} \leqslant 0.5$ (Campbell, 2002; Pierce et al., 2002). For higher values of sliding friction, the bulk friction becomes nearly independent of this parameter. Our tests here are constant normal force instead of constant solid fraction, but the values we used in the simulation were less than 0.5, we therefore tested five different cases, with $\mu_{p-p} = \mu_{p-w} = 0.2$, 0.4, 0.6, 0.8 and 1.0. The results are shown in Fig. 10 for the case of a normal load of 37.83 N and a rotation speed of 120 rpm. In this figure, it can be seen that sliding friction has little effect on the bulk friction behavior for the constant normal force case. The average resisting torque values for strain = [40,50] are 1.77, 1.76, 1.75, 1.82 and 1.75, respectively, for $\mu_{p-p} = \mu_{p-w} = 0.2$, 0.4, 0.6, 0.8 and 1.0.

All of the curves in Fig. 10 show high resisting torque at the beginning. As the shear motion progressed the resisting torque dropped to a steady state. We believe that force

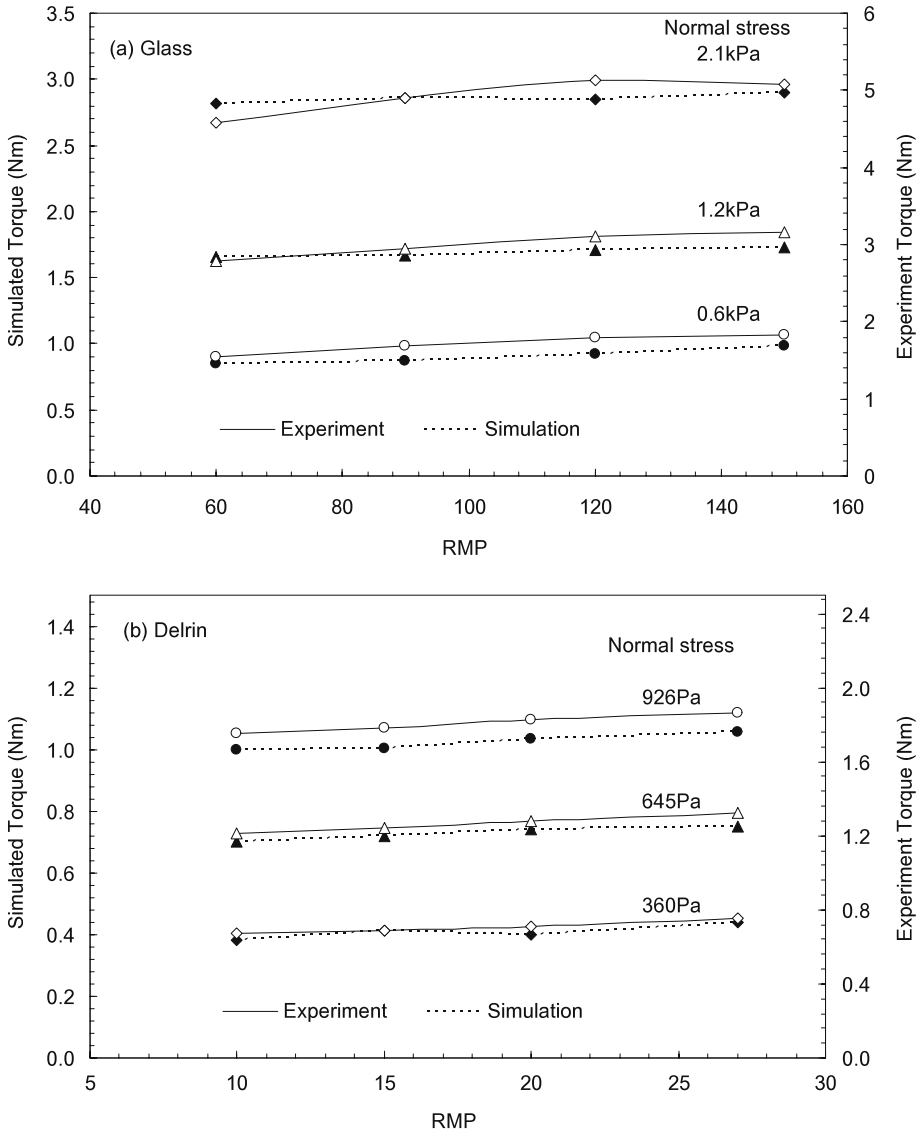

Fig. 9. Comparison between simulated torque and physical test with multi-sized glass and Delrin particles. Left vertical scale for simulation and right for experimental results.

chains formed inside the shear cell initially. When these force chains collapse, the stress is released to lower the bulk resistance. If this hypothesis is correct, the force chain would be stronger for higher friction cases. It is thus expected that the collapse of these force chains is more difficult when contact friction increases, leading to higher peak stress and less number of peaks. However from Fig. 10, neither the peak stress nor the frequency of peaks before steady state seem to depend on the sliding friction. More detailed analysis is therefore required to determine the mechanisms dominating the pre-steady state period.

5.4. Rolling friction

So far, the results obtained do not include rolling friction. As shown in Ting et al. (1989) retarding particle rotation can produce more realistic internal friction and bulk shear modulus for a 2D granular material. Although their simulation employed an artificially increased particle moment of inertia to retard rotation, its results strongly suggested the importance of accounting for rolling friction. Contact models considering rolling friction between particles have been proposed by Sakaguchi et al. (1993) and Iwashita and Oda (1998, 2000). With rolling friction, the additional torque under particle's elastic deformation can be considered to model the particle rotation more accurately. The rolling friction is modeled as follows (Iwashita and Oda, 1998, 2000).

$$M_{\mathrm{r}} = \min\left(K_{\mathrm{r}}\theta + C_{\mathrm{r}}\dot{\theta}, \eta F_{\mathrm{n}}\right) \tag{4}$$

where K_r is the rolling stiffness, C_r is the viscosity coefficient for rolling motion, θ is the relative particle rotation, η is the coefficient of rolling friction. In the above, the parameters are set as

$$K_{\mathrm{r}} = K_s r^2, \quad \eta = \zeta B \tag{5}$$

where K_s is the shear stiffness, r is the particle radius, B is half of the diameter of the contact area, ζ is a non-dimensional parameter, and was set as 0.0, 1.0 or 5.0 in the studies of Iwashita and Oda (1998, 2000). The contact area is calculated from particle overlaps. The rolling viscous coefficient C_r was set as a constant in the studies of Iwashita and Oda (1998, 2000), but in Jiang et al. (2005) it was set as

$$C_r = \frac{C_n B^2}{12} \tag{6}$$

where C_n is the normal viscous coefficient.

By including the rolling friction, Iwashita and Oda (1998, 2000) showed that they were able to produce much better comparisons between the simulation and the physical data for a tri-axial test. These comparisons were limited to kinematics variables as before. No force comparison was reported. The extremely loose packing discovered within the shear band absent from previous DE simulations was found to be successfully reproduced when rolling friction was included in the simulations.

Considering the rolling friction and setting the parameters $\zeta = 3.0$, $C_r = 0$ for glass particles, one test was carried out with a normal load of 67 N and the rotation speed 150 rpm. The comparison with and without rolling friction is given in Fig. 11. In the range of shear strain [60,80], the averaged torques are 3.28 and 4.43 Nm for without and with rolling friction, respectively. The measured value under this condition from the physical experimental was 5.08 Nm. Hence with rolling friction the simulated result is now much closer to the measured value. With the same rolling friction parameters described above, the other cases were also simulated for glass and Delrin particles, and the comparisons between simulated and physical data are given in Fig. 12. Comparing Fig. 12 with Fig. 9 we find that the rolling friction can increase the simulated torque by about 50%. The simulated results of Delrin particles are in better agreement with the physical data than the glass particles. It is noted that these data are based on an artificially chosen parameter $\zeta = 3.0$.

We have also investigated the velocity profile inside the shear cell to see if the local shear rate is different between cases with and without rolling friction. The results of this investigation are given in the Appendix. We observe only very slight increase of local shear rate with the inclusion of the rolling friction. Therefore the increase of bulk

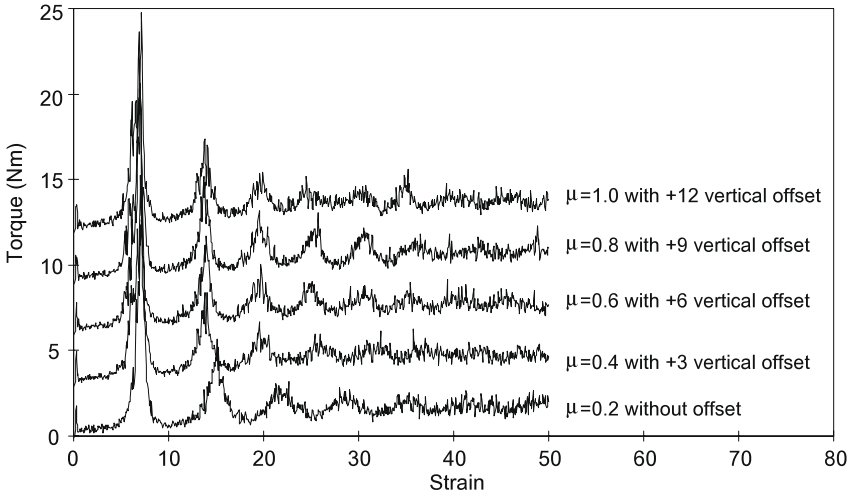

Fig. 10. Comparison of different sliding friction coefficients.

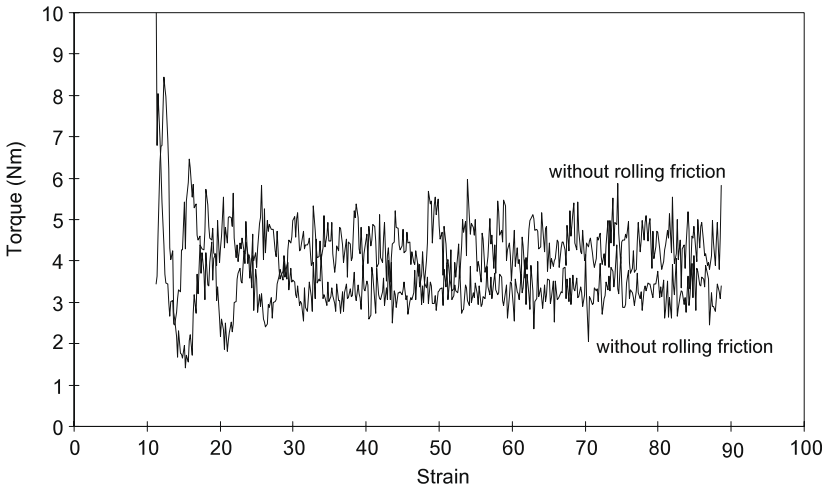

Fig. 11. Comparison of results from contact models with and without rolling friction.

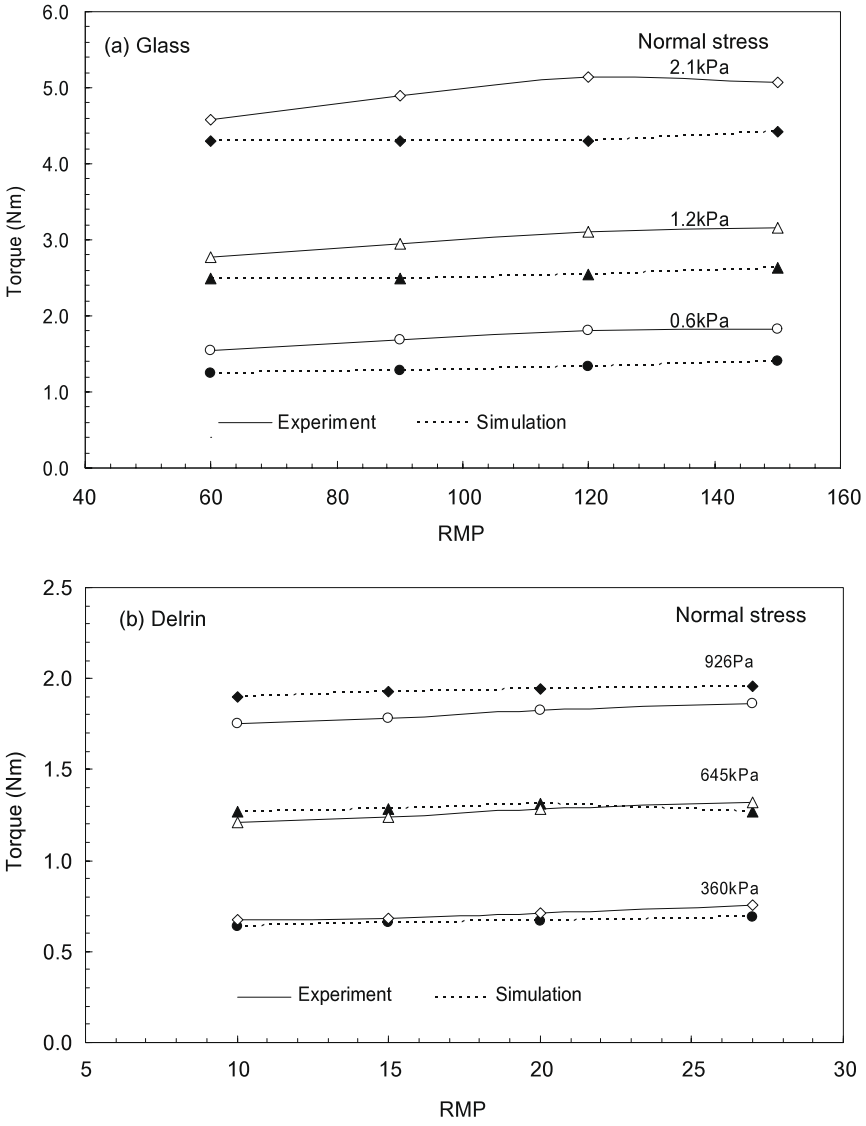

Fig. 12. Comparisons of physical test results with simulated data with rolling friction.

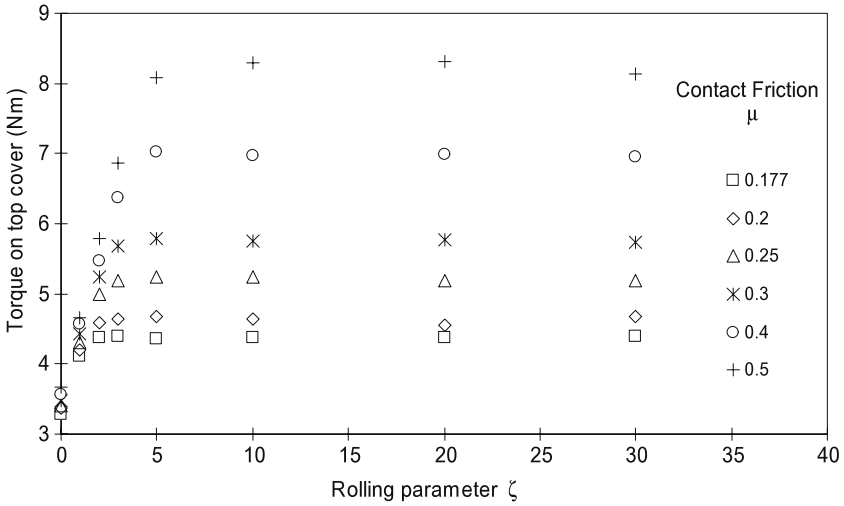

Fig. 13. Combined effect of sliding and rolling friction on the resisting torque. In which $\mu = 0.177$ represents the case $\mu_{p-p} = 0.177$, $\mu_{p-w} = 0.2$ and $\mu = 0.5$ represents the case $\mu_{p-p} = \mu_{p-w} = 0.5$. All other parameters are identical as given in Table 1.

friction when particle's rolling friction is considered is mainly due to the change in shearing force and not the enhanced shear rate.

5.5. Contact force model

In the above, we adopted a linear spring and dashpot model for the contact force. It is known that at least for isotropic elastic spheres, the contact force is not linearly dependent on the normal deformation. From the Hertz theory, the normal contact force is

$$F = K_n^{NL}\delta^{3/2}, \quad K_n^{NL} = \frac{1}{3}\frac{E\sqrt{D}}{(1-\nu^2)} \tag{7}$$

In the above, ν is the Poisson ratio of the particle (Hertz, 1882). This contact force model is obviously very different from the linear model. Based on the numerical study of a simple shear flow of granular materials, the nonlinear contact force model produces qualitatively similar results with that of the linear model (Ji and Shen, 2006). Quantitatively the resulting bulk friction values are different but they do not appear to account for the 100% difference as seen in Figs. 4 and 5. However, when compounded with the rolling friction it is possible that a nonlinear contact model may further improve the comparison between the physical test results and the numerical simulation data. Furthermore, in Ji and Shen (2006) the tangential contact force was very simple. In which the elastic part was assumed to follow the identical model as the normal contact and the tangential viscous damping was set to zero. The complex tangential contact as discussed in Mindlin and Deresiewicz (1953) was not investigated. Further study is required to thoroughly investigate these effects.

5.6. Combining sliding and rolling friction effects

Finally, we tested the combined effect of rolling and sliding coefficients. Fig. 13 shows the results from the case

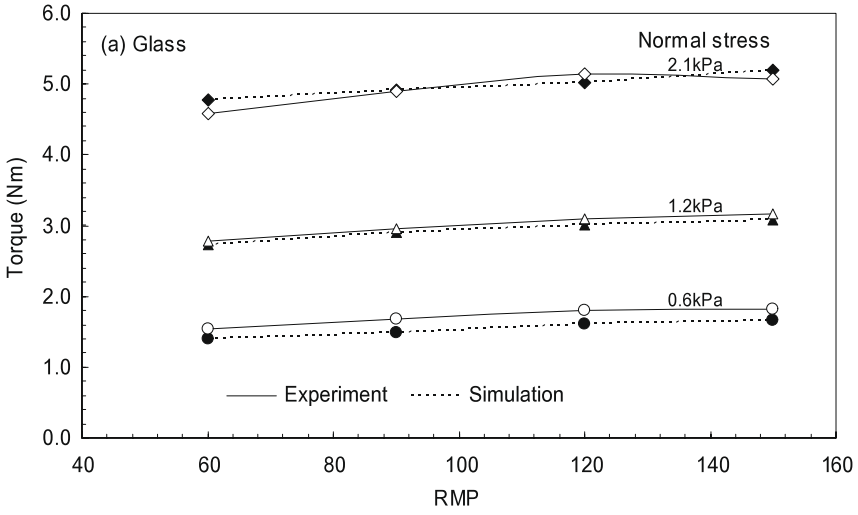

Fig. 14. Comparisons of physical test results with simulated data with $\mu_{p-p} = 0.25, \varsigma = 3$ and other parameters identical to the case shown in Fig. 12(a). Solid lines are from the experiment and dashed lines are from simulations.

with glass particles under 2.1 kN of normal load and 150 rpm rotation. When the rolling friction is zero, increasing the sliding friction from 0.177 to 0.5 only increased the resisting torque from 3.29 to 3.66, but when $\zeta = 5$ the increase between $\mu = 0.177$ and 0.5 is significant, from 4.35 to 8.08. Similar to sliding friction, the effect of rolling friction also approaches an asymptote at large values of ζ. Fig. 14 shows the combination of sliding and rolling friction, assuming both remain constant, for the full range of normal load and shearing rate as tested in the glass particle case shown in Fig. 12(a). In this case, we let $\mu_{p-p} = 0.25$, $\zeta = 3$ and all other parameters identical as given in Table 1. The comparison between the experimental and the simulated results is much improved. It is possible that after repeated use, surface erosion might change the frictional properties of materials. Glass being highly susceptible to wear may explain the need of increased sliding friction even though the value in Table 1 is obtained from "spent" glass.

In this study, serendipitously we also investigated the influence of the mass of the top cover. It was found that this mass had no influence on the steady state torque as long as the normal load was kept the same by the counterweight. In the transient part of the shear, the higher the mass, the higher the peak torque and more delayed is the collapse of the peak. It is also more difficult to reach steady state when the top cover has a higher mass. We increased the mass of the top by a factor of 2 and 3. The results are shown in Fig. 13. The resisting torques when averaged over strain = [60,90], i.e. in the steady state portion, are 1.68, 1.67 and 1.65 Nm for 1, 2 and 3 times of the original mass, respectively. The periodic ups and downs again suggest large force chains forming and breaking inside the shear cell. The magnitude of these ups and downs, and the steady state torque both increase with the mass of the top cover. This phenomenon suggests that in conducting annular shear cell experiments it is easier to reach steady state and protect the integrity of the particles if we use smaller mass for the top cover (Fig. 15).

6. Conclusions

In this study, we present a direct comparison between a physical experiment and a parallel computer simulation of an annular shear cell. In the experiment, the annular shear cell was filled with particles at the beginning. A prescribed normal load was applied and then the bottom of the shear cell began to rotate at a given speed. The top boundary was held stationary in the horizontal direction but free to move up and down. The resisting torque measured at the top boundary was compared between the physical experiment and the computer simulation. Two materials were tested: glass and Delrin. A range of shear speed and normal stress were investigated. The simulated torque is about 1/2 of the measured value over the entire range of shear speed and normal stress if we assume mono-sized spherical particles with simple linear contact model with sliding friction only. The influences of stiffness, boundary packing, particle size distribution, sliding and rolling friction and damping coefficient, and contact force model are discussed. The parameters above except rolling friction have little effect on the simulated torque. Considering rolling friction with the model established by Iwashita and Oda (1998, 2000), the simulated torque values approach the physical data. The remaining discrepancies may come from the compounding effect of all of the above factors.

The present study provides a direct comparison between DE simulations and a physical experiment, including the force measurements. We are encouraged by the consistency of the data over a wide range of parameter space. It is clear that for dense systems as investigated here, not all particle level information is equally influential in simulating the shearing response. However, the friction characteristics are very important to match the forces measured in the physical system.

Acknowledgement

This study is supported by NASA microgravity fluids program, Grant No. NAG3-2717.

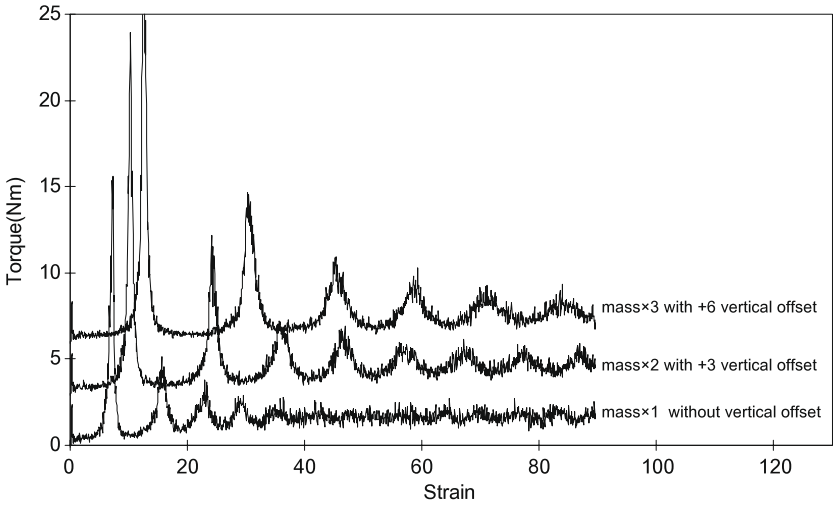

Fig. 15. The comparison of results from top mass equals to the original value of 7.89 kg and equals to 2 and 3 times the original value.

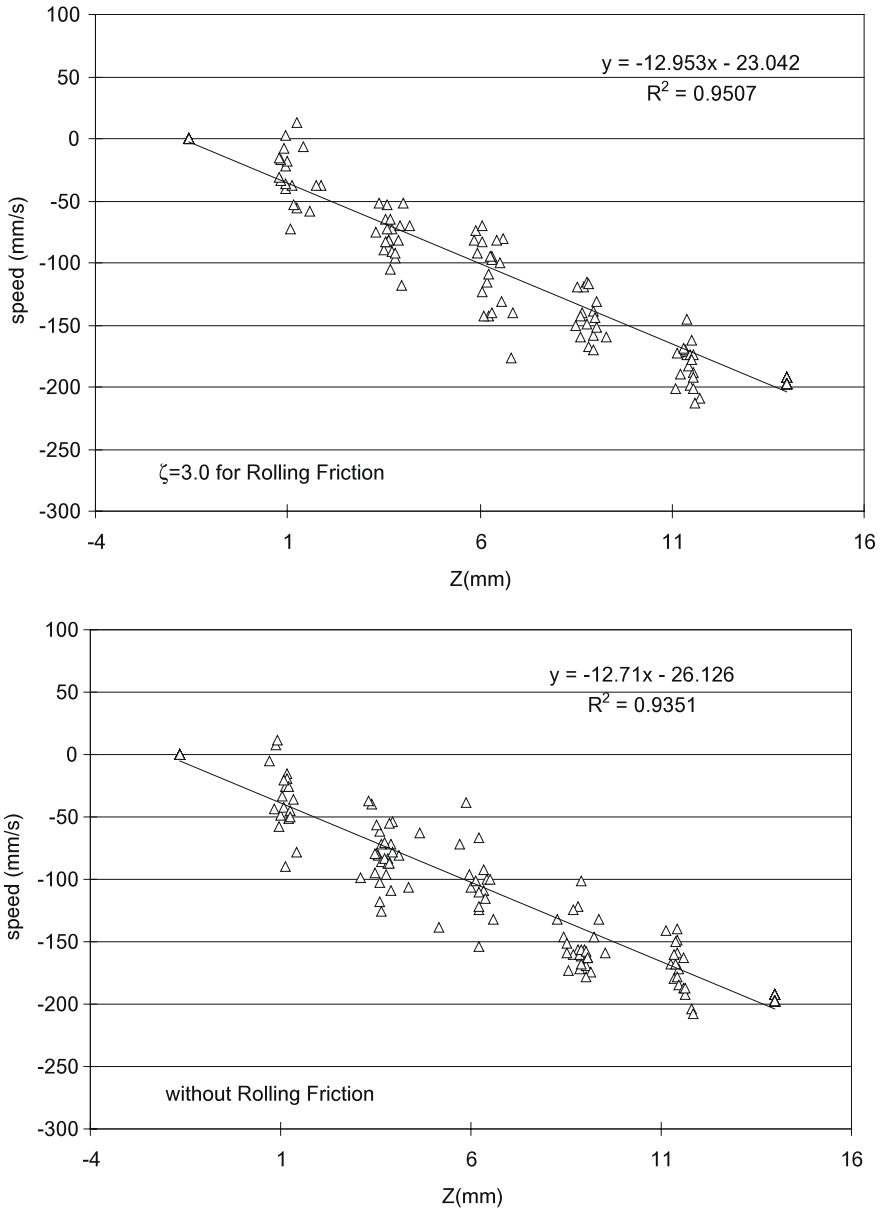

Fig. 16. Particle velocity at different depth inside the shear cell. Note the top is fixed with 0 velocity and the bottom moves with linearly increasing radial velocity.

Appendix A

We consider the case shown in Fig. 11. The velocity of the particles in the center of the shear cell, i.e. those with center of mass located at $\pm D_p$ of $(r_1 + r_2)/2$ are plotted in Fig. 16.

The best-fit line for the case without friction has a slope of -12.71 and for the case with rolling friction coefficient of $\zeta = 3.0$ is -12.95. Hence the "local" shear rate is very close to the estimated value using wall speed and gap size and nearly independent of the rolling friction.

References

Azanza, E., Chevoir, F., Moucheront, P., 1999. Experimental study of collisional granular flows down as inclined plane. Journal of Fluid Mechanics 400, 199–227.

Babic, M., Shen, H.H., Shen, H.T., 1990. The stress tensor in granular shear flows of uniform deformable disks at high solids concentrations. Journal of Fluid Mechanics 219, 81–118.

Bagnold, R.A., 1954. Experiments on a gravity-free dispersion of large solid spheres in a Newtonian fluid under shear. Proceedings of the Royal Society of London Series A: Mathematical and Physical Sciences 225, 49–63.

Campbell, C.S., 1993. Boundary interactions for two-dimensional granular flows, part II: roughened boundaries. Journal of Fluid Mechanics 247, 137–156.

Campbell, C., 2002. Granular shear flows at the elastic limit. Journal of Fluid Mechanics 465, 261–291.

Cleary, P.W., Morrisson, R., Morrell, S., 2003. Comparison of DEM and experiment for a scale model SAG mill. International Journal of Mineral Processing 68, 129–165.

Craig, K., Buckholz, R.H., Domoto, G., 1987. Rapid shear flow of a dry magnetic powder in an externally applied magnetic field: an experimental study. Physical Fluids 30 (7), 1993–1999.

Cundall, P., Strack, O., 1979. A discrete numerical model for granular assemblies. Geotechnique 29, 47–65.

Foerster, S.F., Louge, M.Y., Chang, H., Allia, K., 1994. Measurements of the collision properties of small spheres. Physical Fluid 6 (3), 1108–1115.

Hanes, D.M., Inman, D.L., 1985. Observations of rapidly flowing granular fluid mixtures. Journal of Fluid Mechanics 150, 357–380.

Hanes, D.M., Walton, O.R., 2000. Simulation and physical measurements of glass spheres flowing down a bumpy incline. Powder Technology 109, 133–144.

Hertz, H., 1882. Uber die Beruhrung fester elasticcher Korper (on the contact of elastic solids). Journal fur die Reine und Angewandte Mathematik 92, 156–171.

Howell, D.W., Behriger, R.P., Veje, C.T., 1999. Fluctuations in granular media. Chaos 9 (3), 559–572.

Hsiau, S., Jang, H., 1998. Measurements of velocity fluctuations of granular materials in a shear cell. Experimental Thermal and Fluid Science 17, 202–209.

Iwashita, K., Oda, M., 1998. Rolling resistance at contacts in simulation of shear band development by DE. Journal of Engineering Mechanics 124 (3), 285–292.

Iwashita, K., Oda, M., 2000. Micro-deformation mechanism of shear banding process based on modified distinct element method. Powder Technology 109, 192–205.

Ji, S., Shen, H.H., 2006. Effect of Contact Force Models on Granular Flow Dynamics. ASCE Journal of Engineering Mechanics 132 (11), 1252–1259.

Jiang, M.J., Yu, H.-S., Harris, D., 2005. A novel discrete model for granular material incorporating rolling resistance. Computers and Geotechnics 32, 340–357.

Jop, P., Forterre, Y., Pouliquen, O., 2006. A constitutive law for dense granular flows. Nature 441 (8), 727–730.

Ladipo, D.D., Puri, V.M., 1997. Computer controlled shear cell for measurement of flow properties of particulate materials. Powder Technology 92, 135–146.

Lorenz, A., Tuozzolo, C., Louge, M.Y., 1997. Measurements of impact properties of small, nearly spherical particles. Experimental Mechanics 37 (3), 292–298.

Luding S., 2006. Comparison of ring shear cell simulations in 2d/3d with experiments. In: Proceedings of World Congress Particle Technology, ISBN 0-8169-1005-7, Florida, USA.

Miller, B., Hern, C.O., Behringer, RP., 1996. Stress fluctuations for continuously sheared granular materials. Physical Review Letters 77 (15), 3110–3113.

Mindlin, R.D., Deresiewicz, H., 1953. Elastic spheres in contact under varying oblique forces. ASME Journal of Applied Mechanics 20, 327–344.

Mueth, D.M., Debregeas, G.F., Karczmar, G.S., 2000. Signatures of granular microstructure in dense shear flow. Nature 406, 385–389.

Pierce M, Cundall P, van Hout G., 2002. PFC3D modeling of caved rock under draw. In: International PFC Symposium, Gelsenkirchen, Germany.

Pouliquen, O., 1999. On the shape of granular fronts down rough inclined planes. Physics of Fluids 11 (7), 1956–1958.

Qin H., 2000. Flow Behavior of Granular Materials: Quasi-Static to Inertial Transition. Thesis of Science Master, The University of Florida, 2000.

Sakaguchi, H., Ozaki, E., Igarashi, T., 1993. Plugging of the flow of granular materials during the discharge from a silo. Journal of Modern Physics B 7, 1949–1963.

Savage, S.B., Sayed, M., 1984. Stresses developed by dry cohesionless granular materials sheared in an annular shear cell. Journal of Fluid Mechanics 142, 391–430.

Ting, J.M., Corkum, B.T., Kaufman, C.R., Greco, C., 1989. Discrete numerical modeling for soil mechanics. Journal of Geotechnical Engineering 115, 379–398.

Tsai, J.C., Gollub, J.P., 2004. Slowly sheared dense granular flows: crystallization and nonunique states. Physical Review E 70, 031303.

Vanel, L., Caudin, P.H., Ph, BouchaudJ., et al, 2000. Stresses in silos: comparison between theoretical models and new experiments. Physical Review Letters 84 (7), 1439–1442.

Venugopal, R., Rajamani, R.K., 2001. 3D simulation of charge motion in tumbling mills by the discrete element method. Powder Technology 115, 157–166.

Yang, S.C., Hsiau, S.S., 2001. The simulation and experimental study of granular materials discharged from a silo with the placement of inserts. Powder Technology 120, 244–255.

Zhang, D.Z., Rauenzahn, R.M., 2000. Stress relaxation in dense and slow granular flows. Journal of Rheology 44 (5), 1019–1041.